Chapter 6

Light Sheet-Based Imaging and Analysis of Early Embryogenesis in the Fruit Fly

Khaled Khairy, William C. Lemon, Fernando Amat, and Philipp J. Keller

Abstract

The fruit fly is an excellent model system for investigating the sequence of epithelial tissue invaginations constituting the process of gastrulation. By combining recent advancements in light sheet fluorescence microscopy (LSFM) and image processing, the three-dimensional fly embryo morphology and relevant gene expression patterns can be accurately recorded throughout the entire process of embryogenesis. LSFM provides exceptionally high imaging speed, high signal-to-noise ratio, low level of photoinduced damage, and good optical penetration depth. This powerful combination of capabilities makes LSFM particularly suitable for live imaging of the fly embryo.

The resulting high-information-content image data are subsequently processed to obtain the outlines of cells and cell nuclei, as well as the geometry of the whole embryo tissue by image segmentation. Furthermore, morphodynamics information is extracted by computationally tracking objects in the image. Towards that goal we describe the successful implementation of a fast fitting strategy of Gaussian mixture models.

The data obtained by image processing is well-suited for hypothesis testing of the detailed biomechanics of the gastrulating embryo. Typically this involves constructing computational mechanics models that consist of an objective function providing an estimate of strain energy for a given morphological configuration of the tissue, and a numerical minimization mechanism of this energy, achieved by varying morphological parameters.

In this chapter, we provide an overview of in vivo imaging of fruit fly embryos using LSFM, computational tools suitable for processing the resulting images, and examples of computational biomechanical simulations of fly embryo gastrulation.

Key words Light sheet microscopy, Computational modeling, Tissue biomechanics, Live imaging, Quantitative developmental biology, *Drosophila melanogaster*, Embryonic development, Image processing

1 Introduction

Morphogenesis is a dynamic—inherently three dimensional—process, through which tissues and organs take their shape. In particular, the basic body plan of the developing organism is determined during gastrulation, which can be regarded as a sequence of epithelial tissue invaginations. Such folds are

Celeste M. Nelson (ed.), *Tissue Morphogenesis: Methods and Protocols*, Methods in Molecular Biology, vol. 1189,
DOI 10.1007/978-1-4939-1164-6_6,

ubiquitous in metazoans and uncovering their mechanisms is of wide-reaching importance. For the study of epithelial invaginations, the fruit fly is highly suitable because of its amenability to genetic manipulation. However, our understanding of gastrulation, and morphogenetic processes in general, is limited by the quality and spatial resolution of images we are able to acquire of the process (for both wild type and mutants), the invasiveness and speed of image acquisition techniques, the accuracy by which we can extract phenotypic and dynamic features from the images, and the predictive power of computer simulations that challenge morphogenetic hypotheses.

Compared to conventional microscopy techniques, such as confocal laser scanning microscopy, light sheet fluorescence microscopy (LSFM) is in an excellent position to address the challenges related to image quality, acquisition speed, and invasiveness of the recording process. The key concept behind LSFM is sample illumination in a thin volume section orthogonal to fluorescence detection. Through this arrangement (Fig. 1a, b), LSFM illuminates only the in-focus plane, thus providing intrinsic optical sectioning. This means that it enables simultaneous detection of the fluorescence signal from an entire plane. As a result of this microscope design, LSFM provides high acquisition speed, high signal-to-noise ratio, minimal levels of photo-bleaching, and good penetration depth. The sample typically resides in a low-concentration agarose cylinder (Fig. 1c), which represents a low-stress environment compared to the conventional glass slide/coverslip systems. All of these properties make LSFM particularly suitable for in vivo imaging applications. In the following, we discuss in particular opportunities in the live imaging and study of embryonic development of the fruit fly (Fig. 1d).

The images provided by LSFM contain information on the fluorescently labeled structures in three dimensions and over time, and must typically be appropriately processed before further quantitative analyses are possible. Common requirements are the extraction of nuclear positions, cell boundaries, tissue outlines, cell tracks, and relative label expression levels. The main computational tasks are accordingly image pre-processing, image segmentation, and cell tracking.

Here, we provide an overview of an advanced LSFM system (with simultaneous multiview imaging capability) as applied to the live imaging of fly embryos, and the challenges met for that specific system. We also describe computational tools suitable for processing the resulting LSFM data. Finally, we describe efforts at modeling the mechanics of fly embryogenesis, highlighting current challenges and directions.

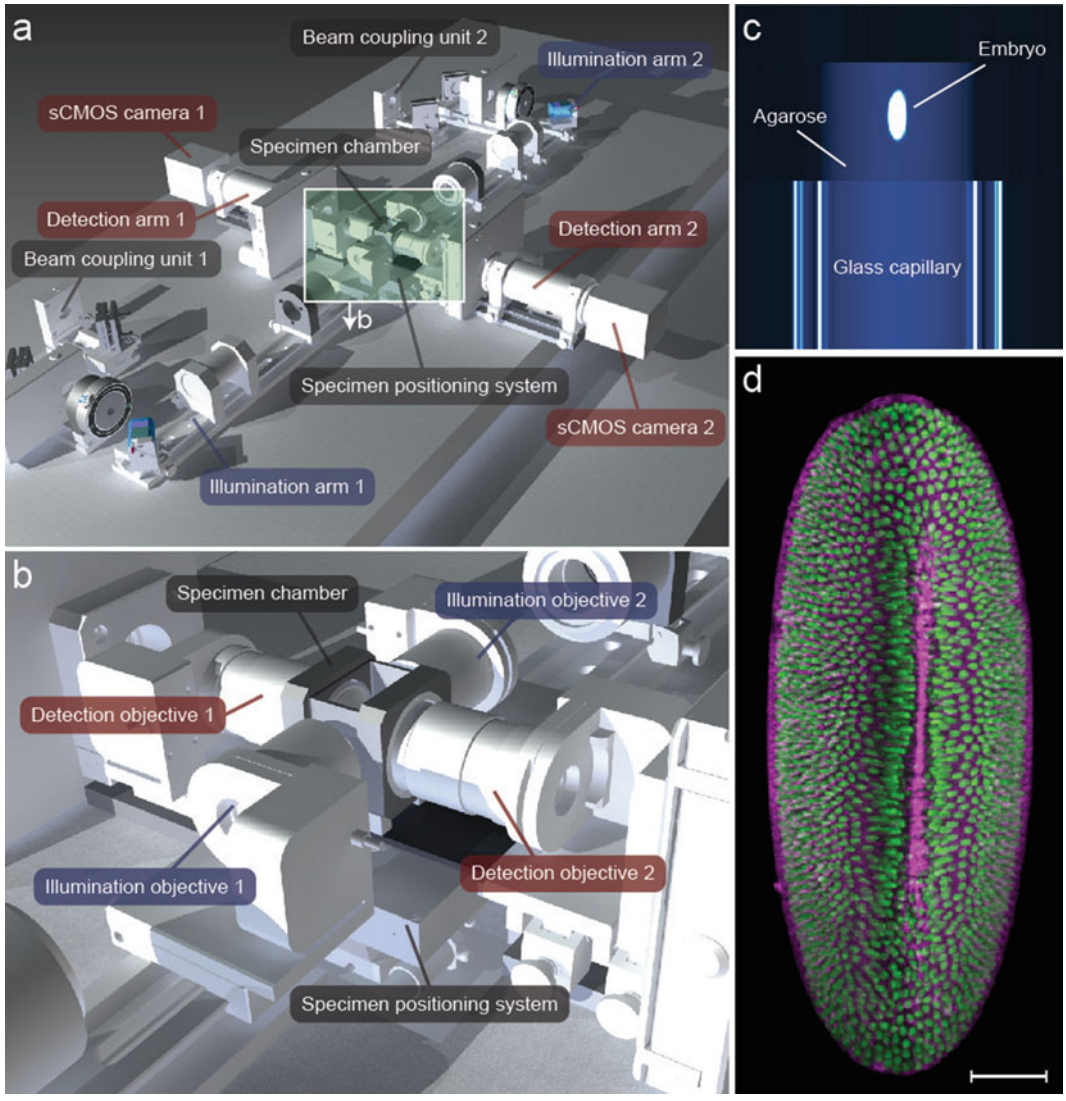

Fig. 1 Multiview light sheet microscopy of fruit fly embryo. (**a**) Layout of SiMView microscope. Two illumination arms generate the scanned laser light sheets used to excite fluorescence in the specimen located in the center of the water-filled specimen chamber. The two detection arms image the emitted fluorescent light onto the chips of high-speed sCMOS cameras. (**b**) Close-up of the specimen chamber in (**a**). (**c**) *Drosophila* embryos are held in the specimen chamber in a vertically oriented cylinder of 1 % agarose. (**d**) Maximum-intensity projection of a SiMView recording of a *Drosophila* embryo (ventral view). Fluorescent labels: nuclei (*green*) and membrane (*magenta*). The snapshot represents one time point of a 24-h long time-lapse recording. Scale bar = 50 μm. Panels (**a**) and (**b**) reprinted from Tomer et al. [14] with permission from Macmillan Publishers Ltd.

2 Materials

2.1 Materials for Fly Embryo Collection and Embedding

1. Grape juice plates (60 mm plastic tissue-culture dishes containing 3 % agar in 50 % grape juice).
2. Yeast paste (1 g of yeast mixed with 1.3 mL of tap water).
3. *Drosophila* mating cages (59-100, Genesee Scientific, Inc.).
4. Mesh basket (46-101, Genesee Scientific, Inc.).
5. Bleach (Sodium Hypochlorite, 425044-1L, Sigma-Aldrich).
6. 1 % low melting temperature agarose (Type VIIa, A0701, Sigma-Aldrich) in tap water.
7. Glass capillary, 20 mm long, 1.5/2.0 mm inner/outer diameter.
8. Scalpel.

3 Methods

3.1 Light Sheet Microscopy for Simultaneous Multiview Imaging

The last decade has seen many advances in light microscopy. Notably, light sheet microscopy has emerged as a powerful new technique that addresses the fundamental limitations arising from the intrinsic performance trade-offs encountered in conventional methods. In many in vivo imaging experiments, several conflicting key parameters need to be carefully balanced. It is usually desirable to achieve high temporal resolution (i.e., imaging speed), high spatial resolution, high signal-to-noise ratio, low photo-bleaching/toxicity, and good spatial coverage of the specimen [1].

Some implementations of light microscopy provide good overall performance, whereas others excel in one parameter, usually by trading off performance in other parameters. Conventional wide-field fluorescence microscopes provide high imaging speed and good signal-to-noise ratio, but lack optical sectioning capability and are therefore unsuited for three-dimensional imaging. Point-scanning confocal fluorescence microscopes provide good spatial resolution and the intrinsic capability to eliminate scattered light [2], but perform poorly with respect to imaging speed, signal-to-noise ratio, photo-bleaching/toxicity, and penetration depth. Point-scanning two-photon microscopes improve over confocal fluorescence microscopes with respect to penetration depth and usually also photo-bleaching/toxicity [3, 4], but further reduce signal-to-noise ratio and imaging speed. Spinning disk confocal microscopes, which use multiple pinholes simultaneously, provide higher imaging speed than (single-)point-scanning confocal fluorescence microscopes [5], but reduce image quality.

Light sheet microscopes combine an intrinsic optical sectioning capability with high imaging speeds, good signal-to-noise ratio, and

low light exposure of the specimen, and are thus particularly well suited for biological live imaging [6–9]. A strength of this unique combination of capabilities is the possibility to study embryonic development at the system level while preserving the ability to follow cellular processes at the high spatiotemporal resolution required for global cell tracking [1].

In contrast to conventional and confocal epi-fluorescence microscopes, which employ the same lens for fluorescence excitation and detection, light sheet microscopes rely on the principle of sample illumination with a planar light sheet perpendicular to the axis of fluorescence detection [10–12]. The light sheet is coplanar with the focal plane of the fluorescence detection system. Fluorescent molecules are only excited in the illuminated plane, which is recorded in a single step with a camera-based detection system. As a result of this intrinsic optical sectioning capability, photo-bleaching and other types of photoinduced damage are avoided outside the thin, illuminated specimen section. This circumstance gives light sheet microscopes a decisive advantage in the fast imaging of sensitive biological specimens as well as in long-term in vivo imaging experiments [12–16]. Light sheet microscopes are furthermore particularly well suited for "multiview imaging," which refers to the strategy of observing the same specimen along multiple different directions. Thereby, parts of the specimen become visible that would otherwise be hidden or obscured in the observation along a single direction, owing to the limited penetration depth of the light microscope [17].

Basic light sheet microscopy implementations typically use a single light sheet and a single detection arm, oriented at a right angle to the light sheet. As in other forms of light microscopy, this single-view imaging arrangement only reveals a significant fraction of large specimens if these are sufficiently transparent. Unfortunately, most multicellular biological specimens are fairly opaque and thus absorb and scatter significant amounts of light when attempting to penetrate deeper than a few cell layers below the surface. For example, at most 30 % of the volume of an early *Drosophila* embryo is visible in high quality from a single view with this basic imaging strategy [14]. The lipid-rich yolk of the *Drosophila* embryo quickly degrades the profile of the light sheet as it passes through the embryo and also makes it impossible to acquire high-quality images from the far side (with respect to the detection axis) of the embryo. In order to improve physical coverage for whole-embryo imaging experiments, multiple views can be recorded sequentially, by simply turning the specimen in the microscope using a rotary stage. In this sequential multiview imaging mode, several complementary three-dimensional image stacks are acquired and subsequently computationally registered and combined [12, 13].

However, sequential multiview imaging only partially addresses the challenge of imaging a large living biological specimen. Since each sequential acquisition and rotation step takes a certain amount of time—during which development of the specimen continues—the resulting multiview image data set cannot usually be correctly registered. Cells are often highly dynamic and are thus captured in different locations and in different states in the respective overlap regions of the recorded multiview stacks. The resulting registration artifacts lead to mistakes and uncertainty in the subsequent data analysis, in particular when automated segmentation and tracking approaches are involved.

The above limitations are overcome by simultaneous multiview imaging: the SiMView light sheet microscopy platform for simultaneous multiview imaging allows simultaneous acquisition of four complementary views of the specimen for optimal physical coverage and furthermore provides exceptionally high imaging speeds [14]. In order to realize simultaneous multiview imaging, SiMView uses an orthogonal arrangement of four independently operated optical arms (Fig. 1a, b). One pair of these opposite arms is used for bidirectional light sheet illumination with two long-working distance air objectives, similar to the illumination arrangement used in earlier light sheet microscopes [18–20]. The other pair, arranged at a right angle to the first, is used for bidirectional fluorescence detection with high numerical aperture water-dipping objectives and fast scientific complementary metal–oxide semiconductor (sCMOS) cameras.

In SiMView experiments, the time delay of multiview image acquisition is on the order of a few tens of milliseconds when using one-photon excitation (owing to the sequential application of bidirectional illumination) and zero when using multiphoton excitation (owing to the simultaneous application of bidirectional illumination). The truly simultaneous operation of all four optical subsystems of the SiMView microscope is possible when using two-photon excitation, since fluorescence excitation is spatially confined to the focal volume. However, in both scenarios (one-photon and multiphoton SiMView imaging), the time delay of multiview image acquisition is by several orders of magnitude shorter than the time required for cells to move or change their shape on a spatial scale comparable to the spatial resolution of the microscope. SiMView is thus particularly well suited for quantitative live imaging of large developing specimens such as entire *Drosophila* embryos [14].

3.2 Methods for Fly Embryo Imaging

Light sheet-based microscopes often rely on long-working distance water-dipping objectives for fluorescence detection and therefore require sample immersion in an aqueous environment. Moreover, if specimens are subjected to multiview imaging, they must be optically accessible for light sheet illumination and fluorescence

detection from multiple angles. These two requirements often introduce challenges in the sample preparation. We developed protocols for live imaging of the entire fruit fly embryos embedded in agarose gels that fulfill these requirements and allow time-lapse data acquisition in a physiologically relevant context over long periods of time.

3.2.1 Embryo Collection and Embedding

To collect several embryos that are at the same developmental stage, it is necessary to begin with a large population of breeding adults (50–100 females). Placing flies of the correct genotype into a mating cage for 1 h should produce a number of synchronized embryos that are suitable for imaging. The adult flies are briefly anesthetized with CO_2 and placed into the mating cage. The open end of the mating cage is covered with a 60 mm tissue culture plate filled with grape juice agar. The grape juice plate should have a small streak of yeast paste in the center to induce the adult females to lay eggs. The flies are left undisturbed for an hour while embryos are being deposited. After an hour the adult flies are removed, leaving the embryos attached to the grape juice agar.

In order to improve the transparency of the embryos for imaging, the outermost embryonic membrane, the chorion, must be removed. The embryos are dechorionated by briefly exposing them to a 50 % solution of bleach in tap water, which causes the chorion to rupture and releases the embryo into the dilute bleach solution. The bleach solution is added directly to the grape juice agar plate and left for 30 s. The solution containing the dechorionated embryos is then poured into an egg collection basket where the embryos are retained by the fine mesh. The embryos are rinsed with copious amounts of water to remove the bleach. The embryos can be transferred to a clean tissue culture dish by inverting the egg collection basket and rinsing them with a small amount of water.

The SiMView light sheet microscope illuminates the embryo from two opposite directions and acquires images orthogonally with two synchronized detection systems (Fig. 1a, b). This requires that the embryo be optically accessible from all sides, which is accomplished by embedding the embryo in a transparent matrix of low-concentration agarose. For *Drosophila* embryos, a 1 % concentration of low-melting-point agarose provides enough mechanical stability to hold the embryo in place while remaining virtually transparent when submerged in the water-filled recording chamber of the microscope.

Embryos are embedded by filling a 20 mm long glass capillary (1.5/2.0 mm inner/outer diameter) with liquid 1 % agarose at 37 °C. The embryos must be gently lifted from the water-filled tissue culture dish on one tine of sharp dissecting forceps and placed into the agarose through one open end of the glass capillary. The agarose will polymerize quickly as it cools to 32 °C, but while the agarose is still liquid the embryo can be gently moved to orient

it appropriately for imaging. The embryos used for the imaging of gastrulation were oriented with the anterior-posterior axis of the animal parallel to the long axis of the capillary. An effort was also made to keep the embryo in the center of the agarose cylinder so that the optical path length through the agarose was approximately equal for the two illumination objectives and the two detection objectives. As the agarose begins to polymerize, the embryo should be left undisturbed so that it is not damaged by mechanical stresses caused by movement through the solidifying matrix.

Before imaging, the polymerized agarose cylinder is extruded out of the end of the capillary until the entire embryo is outside of the glass capillary. The glass causes substantial reflection and refraction of the light passing through it, so the imaging must be performed through agarose only. The agarose cylinder is pushed out of the glass capillary by filling the end opposite the embryo with a small plug of paraffin film or with a plug of plasticine. As the agarose cylinder is extruded, any excess agarose above the embryo can be removed by cutting it off with a scalpel. Then the cylinder is extruded more, just enough to expose the embryo (Fig. 1c). The result is the shortest possible cylinder of agarose exposed outside the glass that provides a clear optical path to the embryo. This maintains the most mechanical stability that can be provided by the low-concentration agarose. The glass capillary with the extruded agarose cylinder is carefully transferred to the water-filled recording chamber of the light sheet microscope and placed vertically into the capillary holder that is attached to the mechanical stages.

3.2.2 *Image Acquisition*

The details of the design of the SiMView light sheet microscope have been described elsewhere [14]. In brief, the specimen is held in a water-filled chamber surrounded by four microscope objective lenses (Fig. 1a, b). Two illumination lenses focus scanned laser light sheets onto the specimen from opposite sides. At right angles to these lenses are two long-working distance, water-dipping detection objectives that focus the emitted fluorescence onto the chips of two sCMOS cameras. All of the objectives are carried on piezoelectric stages so that their planes of focus can be adjusted with submicron accuracy. The focal planes of the detection arms are adjusted so that they are coplanar with the scanned light sheets and provide two complementary views of the illuminated plane of the specimen. The specimen, carried on mechanical four-axis stages, is stepped through the light sheets. The fluorescent light emitted by the specimen at each plane is detected simultaneously by the cameras and the images are acquired by custom software. After images for each plane are acquired, the stack can be assembled into a three-dimensional representation of the entire specimen.

The SiMView microscope offers several advantages for live imaging of animal development (*see* Subheading 3.1) and has

been applied to live imaging of *Drosophila* embryogenesis at 30-s intervals for 24 h [14]. SiMView microscopy enables the acquisition of time-lapse images with subcellular spatial resolution over a duration that is long enough to encompass the entirety of important developmental events and with the temporal resolution to follow the movements of individual cells.

During the early stages of *Drosophila* embryonic development, the cell cycle is very short and interesting morphogenetic events occur rapidly. For these types of specimens, the SiMView microscope is configured to acquire three-dimensional image stacks at 30-s intervals. The specimen volume is recorded with a lateral resolution of approximately 0.5 μm and an axial resolution of approximately 2.0 μm. At each time point of the time-lapse experiment, SiMView acquires four complementary views of the entire specimen. In many cases, the embryo expresses two different fluorescent proteins (e.g., a nuclear red fluorescent protein and a membrane-bound green fluorescent protein) and the image acquisition must be repeated twice in order to image the two colors separately. This increases the time interval between successive images to 1 min. Alternatively, two types of fluorescent proteins can also be imaged simultaneously by separating the fluorescence emission bands with an appropriate dichroic mirror and recording both spectral bands simultaneously with a pair of cameras in each detection arm [13]. Finally, the specimen can also be rotated so that different surfaces of the embryo (e.g., dorsoventral or lateral) face the cameras, and then the entire image acquisition protocol is repeated. This approach allows rotating the microscope's anisotropic point-spread function relative to the specimen, but further increases the time interval between images. In these most complex studies of early *Drosophila* embryo development, images are typically acquired at 2-min intervals. Each time point comprises two-color z stacks recorded from four orthogonal optical views for two different physical orientations (dorsoventral and lateral), encompassing the entire volume of the embryo with an axial step size of approximately 2 μm (Fig. 1d). Recordings typically terminate when the embryo hatches and the larva crawls out of the field of view. The larva can be transferred to a standard vial of fly food and raised to adulthood.

3.3 Image Processing

Before any analysis of morphogenetic mechanisms can be performed, either at the tissue or the cell levels, basic information such as nuclear positions, membrane boundaries, or gene expression levels need to be estimated from the stacks using image processing techniques. Figure 2a shows a standard pipeline suitable for many types of experiments.

3.3.1 Image Pre-processing

Image pre-processing refers to any image filtering or registration technique that needs to be performed in order to facilitate the extraction of information from the image. In this context, it is

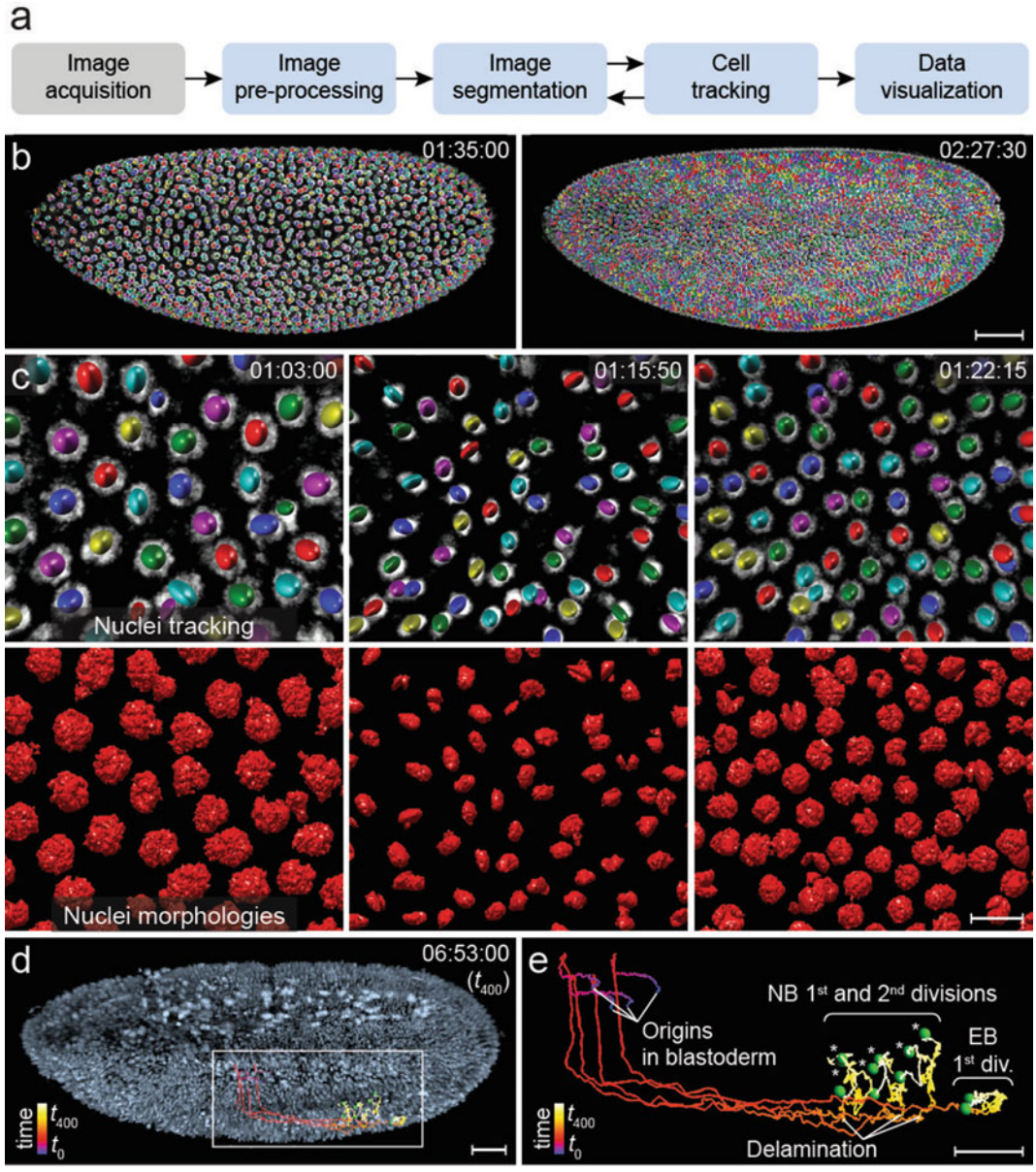

Fig. 2 Image-processing pipeline for SiMView recordings of *Drosophila* embryogenesis. (**a**) Block diagram describing the main steps of a pipeline for obtaining cell lineage information from time-lapse microscopy data. (**b**) Global nuclei tracking in the entire *Drosophila* syncytial blastoderm. Raw image data from light sheet microscopy was superimposed with automated tracking results using a sequential Gaussian mixture model approach. Images show snapshots before the 12th mitotic wave and after the 13th mitotic wave (using a random color scheme in the first time point), which is propagated to daughter nuclei using tracking information. (**c**) Enlarged view of a reconstructed embryo in panel (**a**) with nuclei-tracking information (*left*) and morphological nuclei segmentation (*right*). (**d**) One-photon SiMView recording of a histone-labeled *Drosophila* embryo superimposed with manually reconstructed lineages of three neuroblasts and one epidermoblast for 120–353 min after fertilization (time points 0–400 min); track color encodes time. (**e**) Enlarged view of tracks highlighted in (**c**). *Green spheres* show cell locations at time point 400. *Asterisks* mark six ganglion mother cells produced in two rounds of neuroblast division. *NB* neuroblast, *EB* epidermoblast. Scale bars: 50 μm (**a**), 10 μm (**b**), 30 μm (**c**, **d**). Panels (**b**)–(**e**) reprinted from Tomer et al. [14] with permission from Macmillan Publishers Ltd.

important to take measures to prevent data loss. The choice of specific filters and of the sequence in which they are applied depends on the given task. In the case of multiview image acquisition, the first step is usually to register and fuse all views. Well-tested and freely available tools exist to perform this task automatically and routinely for large-scale LSFM data sets [14, 21, 22]. For visualization purposes, a background subtraction filter is often applied in order to reduce autofluorescence levels and enhance contrast. In cases where dimmer nuclei are located close to more intensely fluorescent ones, median or anisotropic diffusion [23] filtering may be needed to reduce Poisson noise while preserving edges. Finally, it is also common to apply deconvolution algorithms to improve image quality. For this purpose, the Lucy-Richardson algorithm has been shown to be suitable for LSFM data [24]. Care must be taken to prevent the introduction of image artifacts that result from imprecise estimations of the local point-spread function (which can vary substantially across the volume of a large specimen).

Following pre-processing, two key image-processing tasks are frequently performed on time-lapse images of morphogenesis: segmentation and tracking. The former refers to grouping pixels in the same image that correspond to the same object. The latter refers to grouping pixels between images (in time) that correspond to the same objects. These two tasks are classical image processing procedures found in a broad spectrum of problems. They are accordingly strongly represented in the literature. The reader is referred to Khairy and Keller [1] for a survey on recent applications to developmental processes. For imaging fruit fly development, it often suffices to focus on methods for nuclei and membrane markers (Figs. 2a–c). As segmentation and tracking methods group pixels belonging to the same object (one in time and the other in space), these two processes can in principle be interleaved. In other words, a good segmentation makes tracking easier and vice versa.

3.3.2 Nuclei Segmentation

The segmentation of fluorescently labeled nuclei is a blob detection problem, because nuclei morphology is well approximated by an ellipsoid, despite variations in different cell cycle stages. There are four elements that determine the quality of the segmentation and the choice of methodology: the amount of background or autofluorescence present in the sample, the signal-to-noise ratio (SNR), the nuclear size distribution, and nuclear density (number of nuclei per unit image volume).

In that regard, and specifically for *Drosophila*, the yolk core is highly autofluorescent (more so when using GFP, which is excited at around 488 nm), especially in the early stages of development. Therefore, the use of red fluorescent markers is recommended whenever possible. Also image segmentation algorithms need to be tuned to adapt to the different levels of segmentation difficulty

even within one LSFM time-lapse recording. Early in development, nuclei are well separated, but the background (yolk autofluorescence) is high, whereas towards the later stages, the nuclei are more closely packed, with less background signal.

We briefly describe two methods for nuclear segmentation that have been successful for LSFM data and that are freely available. Santella et al. [25] use a difference of Gaussians (Mexican hat) filtering to enhance blobs of pre-specified size. The algorithm assumes that every local maximum from the filter response is the center of a nucleus and uses a machine-learning classifier to remove false detections based on shape features. This approach is very fast and has been tested across different species. In particular, the authors report accuracy rates between 96 and 98 % for different developmental stages of *Drosophila*. However, its performance decreases when nucleus sizes vary significantly and the machine-learning classifier might need retraining to adjust for different image qualities. Moreover, the algorithm returns nuclei centers and radii, instead of a pixel-level segmentation mask. Li et al. [26] presented a method based on diffusion gradient vector flow [27], followed by gradient flow tracking specifically designed to handle scenarios where the nuclei are touching each other. The method returns detailed pixel-level segmentation, but tends to be considerably slower for large 3D datasets. This method has been successfully applied to segmenting fluorescently labeled nuclei in *Drosophila* embryo (Fig. 2c, bottom row).

3.3.3 Membrane Segmentation

The goal of membrane segmentation is to find the boundaries of cells. In images of entire multicellular specimen, cells are touching each other and form a dense network. In general, membrane segmentation is harder than nuclei segmentation due to unevenness in the marker levels across the length of the membrane and the fact that neighboring cells are in direct contact with each other.

There are two common approaches: watershed [28] and active contours (snakes) [29]. The first method is a classical segmentation algorithm that groups "basins" of intensity regions separated by high-intensity contours. Unfortunately, membrane staining tends to be uneven and allows watershed "leaking," which results in merging adjacent cells. Moreover, the watershed method tends to be sensitive to noise. It is thus important to design a good preprocessing strategy to avoid over-segmentation.

The active contour strategy fits a contour by minimizing an energy function with two opposing components: an external and an internal force. The external force comes from the image in the form of edges or intensity gradients. The internal forces regularize the solution in places where the signal is not strong enough or too noisy, thereby preventing the "leakage" effect seen in the watershed algorithm. The regularization is implemented in the form of curvature smoothness, shape constraints, or physical properties of the

tissue. However, it is not straightforward to implement this concept efficiently in 3D images with thousands of connecting active contours.

It is also possible to combine information from both nuclei and membrane channels in order to improve results [30]. For example, a very useful constraint is the fact that only one nucleus can be located per cell. Thus, the nuclei detected can be used to initialize the membrane segmentation using a Voronoi tessellation. Leakage can also be detected if a segmented cell membrane encompasses two nuclei. An important point to consider when using this strategy is that all chromatic aberrations have to be corrected to guarantee proper spatial correspondence between channels.

3.3.4 Tracking

The selection of tracking algorithm depends on the four factors previously discussed in the segmentation scenario (SNR, background intensity, cell density, and size distribution) as well as the temporal resolution of the recording and the spatiotemporal scales of the observed biological process. As a rule of thumb, one should acquire at a rate which guarantees that the structure to be tracked (usually a cell nucleus or a whole cell) has not moved more than half its diameter between consecutive images. Otherwise, accurate tracking and cell division detection can become impossible even for human annotators. For example, during *Drosophila* ventral furrow formation this condition requires acquisition rates faster than 20 s per image stack. Current tracking accuracy rates vary significantly depending on species, imaging technology, and development stage.

Tracking methods can be divided into three categories: contour evolution, state-space models, and data association. Contour evolution is in principle a sequential segmentation in time. The solution at time t is used to initialize a segmentation method, such as snakes, at time $t + 1$. If the temporal sampling is high enough, both time points are similar and the initialization is good enough to allow the segmentation to converge to a good solution. This represents a direct way of combining segmentation and tracking in a single step. Tomer et al. [14] used this approach to track over 3,000 cells in the *Drosophila* blastoderm with 94 % accuracy (Fig. 2b). In this case, the nuclear contours were modeled by ellipsoids forming a Gaussian mixture model on the image intensity that can be propagated in time.

The most common example of state-space models is particle filtering [31]. The user defines a set of parameters that need to be tracked for each nucleus (center, intensity, size, etc.). Given the solution at time t, the tracking algorithm tries to predict the position at time $t + 1$ using a motion model. This prediction is then corrected with the information contained in the image at $t + 1$. A key difference of these methods is that for each parameter a probabilistic distribution is maintained, which returns an estimation of

the uncertainty during the tracking. However, this feature comes at the expense of higher computational complexity, which tends to preclude the use of such approaches in images containing more than a few hundred cells.

Finally, data association methods try to match segmented objects from two time points. Each possible match is given a score based on some similarity measure (size, displacement, etc.). Then the optimal assignment is calculated by generating all matches with maximum score that do not merge tracks. In these cases, the similarity measure is critical to obtain a good solution, as well as a good segmentation method. Kausler et al. [32] presented a data association method specifically tailored to deal with developmental stages presenting many false detections due to background. They showed results in over 256 cells in early *Drosophila* stages with 96 % accuracy rate.

If perfect tracking and segmentation are required, different visualization and editing tools exist to verify results and correct them when necessary. McMahon et al. [33] used Imaris, a commercially available solution, to perform a dynamic analysis of collective cell migrations during gastrulation in *Drosophila*. Tomer et al. [14] also used Imaris to track neuroblast lineages in *Drosophila* (Fig. 2d, e). In addition, Megason [34] and Giurumescu et al. [35] presented freely available tools for cell lineage editing.

3.4 Computational Modeling of the Mechanics of Embryogenesis in the Fruit Fly

To fully understand morphogenesis a thorough investigation of the forces and mechanical responses in the context of the biological tissue must be conducted. Efforts towards this goal meet the challenges of (a) obtaining high spatial and temporal resolution images of fly embryos and relevant gene expression patterns with sufficient spatial coverage and over an adequate time span, (b) obtaining reliable morphological descriptors of the embryo tissue and all cells together with their spatial dynamics through image processing, (c) inferring/uncovering the mechanical effect of action of gene products as well as the mechanical induction of gene expression [36], (d) measuring passive mechanical properties of the tissues, and finally (e) computational modeling to challenge hypotheses. In this section we focus on point (e): the efforts undertaken to model developmental mechanics on a computer, in the context of the fly embryo.

In general, simulations of biomechanical processes require (a) a mathematical morphological description that provides an accurate measure of deformation from a reference shape, (b) a mechanism of applying loads locally to the tissue in accord with the hypothesis under testing, (c) a material constitutive model that represents the mechanical response of the tissue to loads (and together with the extent of deformation provides a shape energy), (d) a method to detect and handle boundaries, and (e) a numerical optimization process to vary the morphological parameters until a minimum energy (predicted) shape is attained.

There is a growing body of literature concerned with modeling the mechanics of morphogenesis. For an excellent recent review the reader is referred to Wyczalkowski and Taber [37]. However, only a small number of works have attempted the simulation of fly embryo mechanics. This is attributed to the difficulty of obtaining high-quality three-dimensional images of developing fly embryos using conventional techniques, and the complete lack of material parameters for epithelial tissues in this system. Those works that considered the mechanics of fly development focused mainly on the process of formation of the ventral furrow invagination, i.e., the sequence of events that leads to the internalization of the future mesoderm cells (the mesoderm primordium). These cells undergo a number of shape changes [38] (Fig. 3a); they constrict apically, and elongate to form an initial furrow. This is followed by cell shortening (at constant cell volume [39]) leading to wedging of the cells at the basal end, i.e., towards the yolk, and the formation of a tubelike structure. The process is known to be driven by the contractility of an actin-myosin meshwork, due to the action of the transcription factors *snail* and *twist* in a ratchet-like mechanism [40].

In a two-dimensional study, Munoz et al. [41, 42] assumed the tissue to be neo-Hookean (i.e., a model that approximates the response of a rubberlike material), consisting of a passive region (located dorsally and laterally), in addition to an active region (ventrally) in which contractile forces are generated. Their finite element numerical treatment is based on an idea of decomposing the deformation gradient tensor (the numerical entity that measures the extent of deformation for all considered deformation modes at a specific material point) into an active and a passive component, and the problem was formulated in terms of strain energy, which was then minimized to obtain predicted shapes. Their continuum model confirmed the notion that several mechanisms act together to provide the necessary robustness to the furrow formation process, and that there exists a set of allowed ratios of apical constriction vs. apicobasal elongation that favor the formation of the furrow as observed in experiments. The extension of this work to three spatial dimensions [43] predicts additional robustness, and the presence of an accordion-like global compression and expansion wave that moves through the embryo due to yolk flow. Both studies underline the importance of the vitteline membrane as a constraint, as well as the yolk volume. In addition the model makes the assumption that cells in the dorsal and lateral regions of the embryo epithelium shorten along their apicobasal axis. This is equivalent to the ectoderm "pushing," thereby facilitating the formation of the invagination. The major numerical difficulty that was overcome in these simulations is the "chatter" that occurs during optimization calculations involving discretized constraint surfaces. This was solved by approximating the vitteline membrane

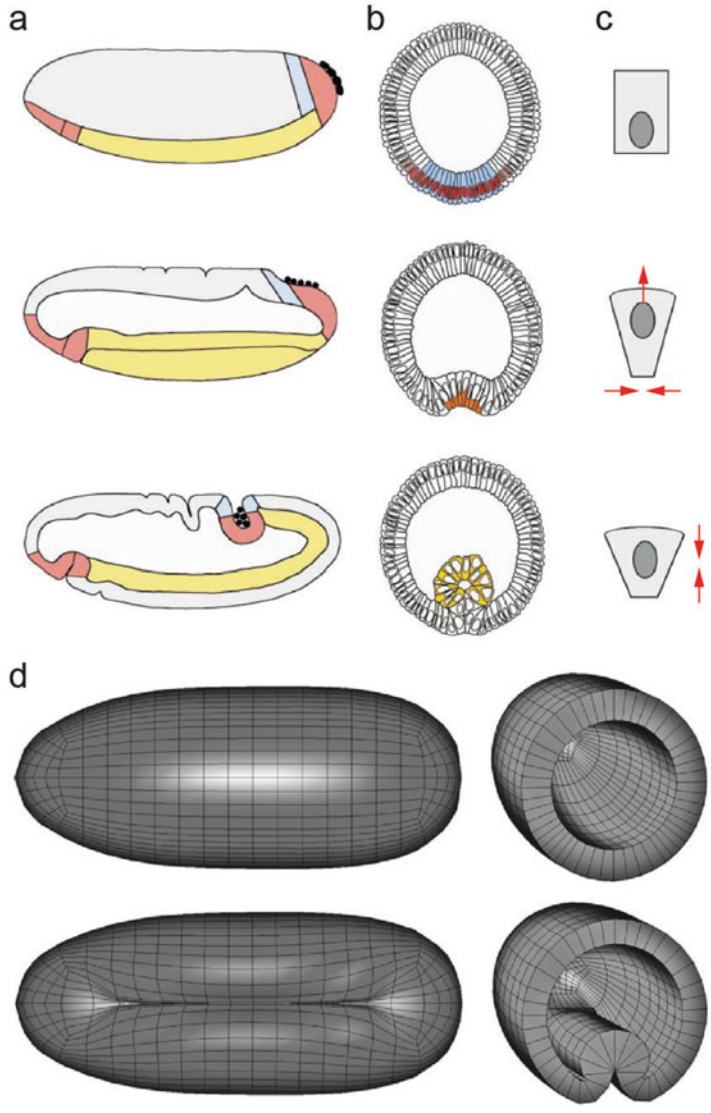

Fig. 3 Cell shape changes during ventral furrow formation and mechanical simulation. (**a**) Drawings of whole embryos indicating the regions of the mesodermal (yellow), endodermal (red), and ectodermal (grey, blue) primordia. At the cellular blastoderm stage (~3 h of development at 25 °C) the primordia lie at the surface of the embryo (*top*). Fifteen minutes later, the prospective mesoderm has formed a furrow on the ventral side of the embryo (*second embryo*). A few minutes later, the posterior part of the endoderm has invaginated and the germ band has begun to extend onto the dorsal side of the embryo (*third embryo*). (**b**) Diagrams of cross sections of embryos at the same stages as those shown in (**a**). Colors mark regions or cells in which events relevant for gastrulation occur. (**c**) Sketch of changes in a mesodermal cell in the embryos shown on the left. (**d**) Finite element simulation of ventral furrow invagination. *Top row*: starting shape. *Bottom row*: computational model result. Panels (**a**)–(**c**) reproduced from Leptin [38] with permission from Nature Publishing Group. Panel (**d**) reproduced from Conte et al. [43] with permission from Elsevier

using cubic B-splines, and incorporating this sliding contact tightly in the optimization iterations [44].

In another study, also using finite elements, the embryo was parameterized by a system of curvilinear coordinates, adopted from potential theory [45], that facilitated its treatment as a thick shell [46]. The authors simulated both the formation of the cephalic furrow and the simultaneous formation of cephalic and ventral furrows.

Ultimately, it is desirable to connect the data collected from microscopy to the mechanics of the underlying tissue. Towards this goal, we mention a strategy that infers forces involved in the ventral furrow formation from fluorescence microscopy images. Brodland et al. [47] used a mechanical model into which strains are input by using segmented images of a section through the embryo to estimate relative forces needed for the induction of such strain using mathematical inverse methods. Forces are assumed to be decomposed into active and passive components. Within a finite element framework, they relied on a general cell-based model [48], in which cell-cell interactions are represented by rod elements (loci for active forces), and the viscosity of the cytoplasm by orthogonal dashpots (passive force components). This approach solves a stiffening artifact that arises when space-filling viscous elements are used to model the cytoplasm. Although their work was conducted on two-dimensional images, it is pioneering in the sense that it analyzes the image data directly in the context of the mechanics of the underlying tissue.

Many of the challenges in embryo mechanics simulations are numerical in nature. The studies above were made possible by meeting (one or more of) these challenges, treating boundary conditions smoothly, choosing the best energy optimization strategy, mathematically representing the embryo morphology adequately, and/or avoiding problem formulations that lead to numerical artifacts and prevent convergence. Overcoming these computational and numerical challenges will open the door to more efficient simulations. However, it must be kept in mind that improvements in the predictive power of embryogenesis mechanics computer simulations in the future will also critically depend on the ability to record higher quality three- and four-dimensional live image data of all relevant structures, accurate estimation of morphology through improved image segmentation and tracking, more realistic biological material models, and accurate experimental material parameter measurements, which are currently lacking for the fly embryo.

Acknowledgments

This work was supported by the Howard Hughes Medical Institute.

References

1. Khairy K, Keller PJ (2011) Reconstructing embryonic development. Genesis 49(7): 488–513
2. Pawley JB (2006) Handbook of biological confocal microscopy. Springer, New York, NY
3. Diaspro A, Chirico G, Collini M (2005) Two-photon fluorescence excitation and related techniques in biological microscopy. Q Rev Biophys 38(2):97–166
4. Helmchen F, Denk W (2005) Deep tissue two-photon microscopy. Nat Methods 2 (12):932–940
5. Graf R, Rietdorf J, Zimmermann T (2005) Live cell spinning disk microscopy. Adv Biochem Eng Biotechnol 95:57–75
6. Keller PJ, Dodt HU (2011) Light sheet microscopy of living or cleared specimens. Curr Opin Neurobiol 22(1):138–143
7. Tomer R, Khairy K, Keller PJ (2011) Shedding light on the system: studying embryonic development with light sheet microscopy. Curr Opin Genet Dev 21(5):558–565
8. Weber M, Huisken J (2011) Light sheet microscopy for real-time developmental biology. Curr Opin Genet Dev 21(5):566–572
9. Mertz J (2011) Optical sectioning microscopy with planar or structured illumination. Nat Methods 8(10):811–819
10. Siedentopf H, Zsigmondy R (1903) Über Sichtbarmachung und Größenbestimmung ultramikroskopischer Teilchen, mit besonderer Anwendung auf Goldrubingläser. Ann Phys 315(1):1–39
11. Voie AH, Burns DH, Spelman FA (1993) Orthogonal-plane fluorescence optical sectioning: three-dimensional imaging of macroscopic biological specimens. J Microsc 170(3): 229–236
12. Huisken J et al (2004) Optical sectioning deep inside live embryos by selective plane illumination microscopy. Science 305 (5686):1007–1009
13. Keller PJ et al (2008) Reconstruction of zebrafish early embryonic development by scanned light sheet microscopy. Science 322(5904): 1065–1069
14. Tomer R et al (2012) Quantitative high-speed imaging of entire developing embryos with simultaneous multiview light-sheet microscopy. Nat Methods 9(7):755–763
15. Arnaout R et al (2007) Zebrafish model for human long QT syndrome. Proc Natl Acad Sci U S A 104(27):11316–11321
16. Scherz PJ et al (2008) High-speed imaging of developing heart valves reveals interplay of morphogenesis and function. Development 135(6):1179–1187
17. Swoger J et al (2007) Multi-view image fusion improves resolution in three-dimensional microscopy. Opt Express 15(13):8029–8042
18. Truong TV et al (2011) Deep and fast live imaging with two-photon scanned light-sheet microscopy. Nat Methods 8(9):757–760
19. Huisken J, Stainier DY (2007) Even fluorescence excitation by multidirectional selective plane illumination microscopy (mSPIM). Opt Lett 32(17):2608–2610
20. Dodt HU et al (2007) Ultramicroscopy: three-dimensional visualization of neuronal networks in the whole mouse brain. Nat Methods 4 (4):331–336
21. Preibisch S et al (2010) Software for bead-based registration of selective plane illumination microscopy data. Nat Methods 7 (6):418–419
22. Rubio-Guivernau JL et al (2012) Wavelet-based image fusion in multi-view three-dimensional microscopy. Bioinformatics 28 (2):238–245
23. Perona P, Malik J (1990) Scale-space and edge detection using anisotropic diffusion. IEEE Trans Pattern Anal Mach Intell 12(7):629–639
24. Lucy LB (1974) An iterative technique for the rectification of observed distributions. Astron J 79(6):745–754
25. Santella A et al (2010) A hybrid blob-slice model for accurate and efficient detection of fluorescence labeled nuclei in 3D. BMC Bioinformatics 11:580
26. Li G et al (2007) 3D cell nuclei segmentation based on gradient flow tracking. BMC Cell Biol 8:40
27. Xu C, Prince J (1998) Snakes, shapes, and gradient vector flow. IEEE Trans Image Proc 7(3):359–369
28. Lin G et al (2003) A hybrid 3D watershed algorithm incorporating gradient cues and object models for automatic segmentation of nuclei in confocal image stacks. Cytometry A 56(1):23–36
29. Dufour A et al (2005) Segmenting and tracking fluorescent cells in dynamic 3-D microscopy with coupled active surfaces. IEEE Trans Image Process 14(9):1396–1410
30. Pop S et al (2013) Extracting 3D cell parameters from dense tissue environments:

application to the development of the mouse heart. Bioinformatics 29(6):772–779

31. Smal I et al (2008) Multiple object tracking in molecular bioimaging by Rao-Blackwellized marginal particle filtering. Med Image Anal 12(6):764–777
32. Kausler BX et al (2012) A discrete chain graph model for 3D + t cell tracking with high misdirection robustness. In: Fitzgibbon A et al (eds) Computer vision - ECCV 2012. Springer, Berlin, pp 144–157. doi:10.1007/978-3-642-33712-3_11
33. McMahon A et al (2008) Dynamic analyses of Drosophila gastrulation provide insights into collective cell migration. Science 322 (5907):1546–1550
34. Megason SG (2009) In toto imaging of embryogenesis with confocal time-lapse microscopy. Methods Mol Biol 546:317–332
35. Giurumescu CA et al (2012) Quantitative semi-automated analysis of morphogenesis with single-cell resolution in complex embryos. Development 139(22):4271–4279
36. Farge E (2003) Mechanical induction of Twist in the Drosophila foregut/stomodeal primordium. Curr Biol 13(16):1365–1377
37. Wyczalkowski MA et al (2012) Computational models for mechanics of morphogenesis. Birth Def Res C Emb Today 96(2):132–152
38. Leptin M (1999) Gastrulation in Drosophila: the logic and the cellular mechanisms. EMBO J 18(12):3187–3192
39. Gelbart MA et al (2012) Volume conservation principle involved in cell lengthening and nucleus movement during tissue morphogenesis. Proc Natl Acad Sci U S A 109(47): 19298–19303
40. Martin AC, Kaschube M, Wieschaus EF (2009) Pulsed contractions of an actin-myosin network drive apical constriction. Nature 457 (7228):495–499
41. Munoz JJ, Barrett K, Miodownik M (2007) A deformation gradient decomposition method for the analysis of the mechanics of morphogenesis. J Biomech 40(6):1372–1380
42. Conte V et al (2009) Robust mechanisms of ventral furrow invagination require the combination of cellular shape changes. Phys Biol 6 (1):016010
43. Conte V, Munoz JJ, Miodownik M (2008) A 3D finite element model of ventral furrow invagination in the Drosophila melanogaster embryo. J Mech Behav Biomed Mater 1 (2):188–198
44. Munoz JJ (2008) Modelling unilateral frictionless contact using the null-space method and cubic B-Spline interpolation. Comput Methods Appl Mech Eng 197:979–993
45. Kellog OD (1953) Foundations of potential theory. Springer, Berlin
46. Allena R, Aubry D (2012) An extensive numerical simulation of the cephalic furrow formation in Drosophila embryo. Comput Methods Biomech Biomed Engin 15(5): 445–455
47. Brodland GW et al (2010) Video force microscopy reveals the mechanics of ventral furrow invagination in Drosophila. Proc Natl Acad Sci U S A 107(51):22111–22116
48. Viens D, Brodland GW (2007) A three-dimensional finite element model for the mechanics of cell-cell interactions. J Biomech Eng 129(5):651–657